Carbon nanotube intermediate layer intercalation and its influence on surface charge of thin film composite membrane

Deng, Luyao ; Gonzales, Ralph Rolly ; Thomas, Joy ; Takagi, Ryosuke ; Fu, Wenming ; Liu, Cheng-Liang ; Xiang, Shang ; Matsuyama, Hideto

(Citation)
Composites Part B: Engineering,289:111951

(Issue Date)
2025-01-15

(Resource Type)
journal article

(Version)
Version of Record

Composites Part B 289 (2025) 111951

Contents lists available at ScienceDirect

Composites Part B

journal homepage: www.elsevier.com/locate/compositesb

Carbon nanotube intermediate layer intercalation and its influence on surface charge of thin film composite membrane

Luyao Deng [a,b,c], Ralph Rolly Gonzales [a,d,**], Joy Thomas [a,e], Ryosuke Takagi [a], Wenming Fu [a,b], Cheng-Liang Liu [e], Shang Xiang [a,b], Hideto Matsuyama [a,b,*]

[a] Research Center for Membrane and Film Technology, Kobe University, Kobe, Japan
[b] Department of Chemical Science and Engineering, Kobe University, Kobe, Japan
[c] Research & Development Department, Shandong Wego Blood Purification Products Co. Ltd, Weihai, China
[d] Scion, Private Bag 3020, Rotorua, New Zealand
[e] Department of Materials Science and Engineering, National Taiwan University, Taipei, Taiwan

ARTICLE INFO

Handling Editor: Dr Hao Wang

Keywords:
Thin film composite (TFC) membrane
Carbon nanotubes
Layered structures
Polyamide

ABSTRACT

The surface charge of a separation membrane is a critical factor affecting its performance in ion separation and fouling resistance. Thin-film composite (TFC) polyamide (PA) membrane, commonly used in water treatment, often suffer from excessive surface negative charges, which significantly limits their application and fouling resistance. To address this issue, this work introduces a carbon nanotubes (CNT) intermediate layer to adjust the surface charge of TFC PA membranes, aiming to achieve a PA layer with neutral properties. Novel grazing-incidence wide-angle x-ray scattering (GIWAXS) measurements were employed to elucidate the effect of CNT on the molecular chain stacking of PA. The CNT intermediate layer was found to influence the PA cross-linking, which is related to surface negative charge, by controlling the storage and release of the *m*-phenylenediamine monomer during interfacial polymerization. The neutral CNT-TFC membrane demonstrated improved NH_4^+ retention and increased resistance to fouling by protein, surfactant, and *E. coli*. However, other surface properties, such as roughness and hydrophilicity, could counteract the antifouling benefits of a neutral surface. This work provides insights into additional advantages of CNT intermediate layer intercalation in TFC PA membranes, such as enhanced cross-linking and surface charge control.

1. Introduction

The exponential growth of the world's population and rapid economic development have led to a significant increase in the demand for clean and accessible water [1,2]. To address the water scarcity crisis, seawater desalination and wastewater reuse are increasingly being employed to provide a fresh and clean water supply [3,4]. Over the past six decades, membrane technology has played a crucial role in water resources and water reuse, due to its less cost and sustainable and efficient solutions in augmentation of water supply [5,6]. Membrane applications have evolved to highly efficient processes not only for desalination, as well as treatment of wastewater and industrial effluents [7].

Reverse osmosis (RO) is a pressure-driven membrane process that has gained extensive recognition and is now being widely employed in various applications, encompassing desalination, selective separation, purification, and concentration processes [8]. RO can separate dissolved solutes, which include monovalent ions like Na^+ and Cl^- and organic molecules with low molecular weights, from water through a semi-permeable membrane that allows water to pass through while selectively blocking solutes. As both research and industrial applications of RO have flourished, new composite membranes have emerged, further enhancing RO's potential for a wide range of applications and improving its capabilities in handling water-related issues.

An excellent membrane material candidate for RO is the thin film composite (TFC) membrane, which typically consists of a porous substrate and an ultrathin selective polyamide (PA) layer prepared using interfacial polymerization (IP) [9]. Both the substrate and selective layers can be modified and controlled separately to achieve the desired properties and performance. The PA selective layer is conventionally

* Corresponding author. Research Center for Membrane and Film Technology, Kobe University, Kobe, Japan.
** Corresponding author. Research Center for Membrane and Film Technology, Kobe University, Kobe, Japan.
E-mail addresses: ralph.gonzales@scionresearch.com (R.R. Gonzales), matuyama@kobe-u.ac.jp (H. Matsuyama).

https://doi.org/10.1016/j.compositesb.2024.111951
Received 27 November 2023; Received in revised form 24 October 2024; Accepted 4 November 2024
Available online 5 November 2024

prepared using the IP reaction of diamines, present in aqueous solutions, and acyl chlorides, present in organic solutions, near the organic phase side of the interface [10,11]. The TFC RO membrane preparation typically employs *m*-phenylenediamine (MPD) and trimesoyl chloride (TMC) as the respective diamine and acyl chloride monomers [12]. The development of TFC membranes has continued to grow due to the exceptional characteristics of the membrane, such as high permeability and selectivity, robustness, and resistance to a wide range of pH, temperatures or foulant adsorption [13,14]. The performance of TFC membranes is mainly determined by the characteristics of the PA thin film, thus finding a facile way to control the PA property is of great importance for improving TFC membrane performance with specific demanding [15,16].

The surface characteristics of TFC membranes, such as roughness, porosity, pore size, exposed membrane surface area, polarity and charge density, are very important to ensure the quality of treatment process and managing surface interactions and foulant deposition mechanisms [17]. For example, the TFC membrane's selectivity and anti-fouling performance largely depend on the charge of its surface, which is consequently influenced by the polarizability of the functional groups at the liquid-solid interface [18]. Many researchers have attempted to customize the charge of membrane surface to achieve efficient separation without sacrificing permeability, especially for treating solutions containing charged substances. Among the methods performed for membrane surface charge engineering in literature include layer-by-layer assembly [19,20], specialized IP process [21], and surface grafting [18,22]. Other earlier work on surface charge control of TFC membranes involve the quenching of residual acyl chloride groups in nascent PA films by secondary IP [23,24] and regulation of the IP process to influence hydrolysis and cross-linking [25,26]. Remarkable changes on surface charge were achieved; however these methods have certain limitations, such as multi-step operation, cumbersome process, and uncontrollable degree and rate of reaction [21]. Therefore, there is a pressing need for a straightforward method to control surface charge.

Kinetic analysis of the IP process has revealed that the reaction occurs very rapidly [27], and the acyl chloride groups in TMC molecules could hydrolyze to carboxyl (–COOH) groups [28]. The surface charge and cross-linking degree of PA become more pronounced with the net content of –COOH groups and the extent of reaction between MPD and TMC. That offers a direct way of surface charge tailoring through influencing the IP reaction. The IP reaction occurs in-situ on the surface of a porous substrate, offering a potential way to influence the IP reaction by adjusting the surface properties of the substrate, thereby regulating the surface charge of formed PA layer [29,30]. Surface properties such as pore size, hydrophilicity and functionalization can be easily tailored through several conventional methods, including but not limited to matrix blending and surface modification.

Particularly, the intercalation strategy using one-dimension nanomaterials, such as carbon nanotubes (CNT), to form a nano-network atop the substrate has become a novel approach to tailor the substrate properties and the structure of TFC membranes [31]. The ability of CNTs to form nano-networks is owed to intramolecular covalent bonds, which also provide CNT outstanding mechanical properties [32–34]. In this method, the CNTs are intercalated as a layer between the PA layer and the substrate in a two-dimensional manner. This CNT intermediate layer has been shown to effectively adjust the surface properties of substrate [35], facilitate water transport through gutter layer effect [36–38], and reduce PA intrusion into the substrate [39,40]. The first attempt to use the CNT intercalation strategy was reported by Marand and Johnson et al. [31] in 2013, who intercalated a network formed by zwitterion-functionalized CNTs between the PA layer and the substrate layer. This CNT intermediate layer, along with the zwitterion functionalization, resulted in a fourfold increase in water flux. Subsequent research has further explored the mechanisms behind the performance enhancement of membranes with a CNT intermediate layer. For example, Hu et al. [39] investigated the backside of PA layer formed on the CNT intermediate layer and found that this CNT layer effectively prevented the growth of PA into the macropores of the substrate. Tang et al. [37,38] studied the gutter layer effect of the CNT intermediate layer through transport modeling and experiments, proving that a highly permeable interlayer can facilitate water transport in the transverse direction, thereby minimizing the transport distance within the low-permeability PA film. In our earlier work, we have investigated the role of CNT intermediate layer in PA formation and we found that the CNT intermediate layer could influence the MPD supply regulation and IP monomer release rate [35]. The CNT coating was proved to decrease the MPD storage capacity and increase the MPD release rate, which ultimately influenced the IP reaction with TMC and ultimately the PA film formation. Based on this, the CNT intermediate layer could be a significant instrument in regulation of the PA surface charge, which could further bring an effect on the membrane performance which are charge-dependent, such as ammonium separation [23,41].

In this work, the influence of CNT intermediate layer on the surface charge of polyketone (PK)-based TFC membranes was investigated, and the feasibility of surface charge regulation using CNT intermediate layer was examined. The resultant neutral CNT-interlayered thin film nanocomposite (CNT-ITFN) membrane was evaluated in both ammonium separation and fouling-resistance performance, which were earlier found to be influenced by the cross-linking degree and surface charge of the PA selective layer [23,41,42]. This work provides insights on other benefits, such as higher cross-linking and surface charge control, of the intercalation modification which are often overlooked during development of TFC membranes.

2. Experimental

In this work, we maintained the same membrane fabrication method as in our previous study [35]. However, the CNT-ITFN membranes were applied to water treatment instead of organic solvent environment to amplify the charge effect on separation performance. Additionally, grazing-incidence wide-angle X-ray scattering (GIWAXS) measurements were applied for the first time to investigate the layered structure of CNT-ITFN membranes. The detailed materials and procedures for membrane preparation, characterization, and evaluation of membrane performance and fouling control ability are shown in the Supporting Information.

3. Results and discussion

3.1. Structure of CNT-ITFN membranes

The surface morphologies of polyketone (PK) and PK-CNT substrates with different CNT loadings were shown and discussed in Fig. S1, with 0.5 mL coating amount determined as the minimum filtration volume of CNT dispersion to prepare a continuous CNT network (Fig. S1c), as observed in earlier studies involving CNT [43].

The influence of CNT intermediate layer on the surface morphology of PA selective layer is shown in Fig. 1a. The pristine TFC membrane (TFC-0) showed the typical ridge-and-valley and nodular structures characteristic of the PA layer (Fig. 1a1). However, upon the introduction of CNT intermediate layer, it could be noticed that the ridge-and-valley structures evolved into larger leaf-like structures, and the nodular structures gradually turned into ridge-and-valley structures. The PA leaf-like structures could also be observed to overlap with each other, resulting in an apparent multi-layered structure.

To further understand the structure of CNT-ITFN membranes, Fig. S2 shows large-scale cross-sectional SEM images of TFC membranes. Since the thickness of the PK substrate is around 100 μm, the overall thickness of the TFC membrane does not change significantly after the IP reaction because the CNT intermediate layer and PA layer are ultrathin and at the nano-level. To differentiate between layers, high-resolution cross-sectional SEM images are presented in Fig. 1b. For all samples, the

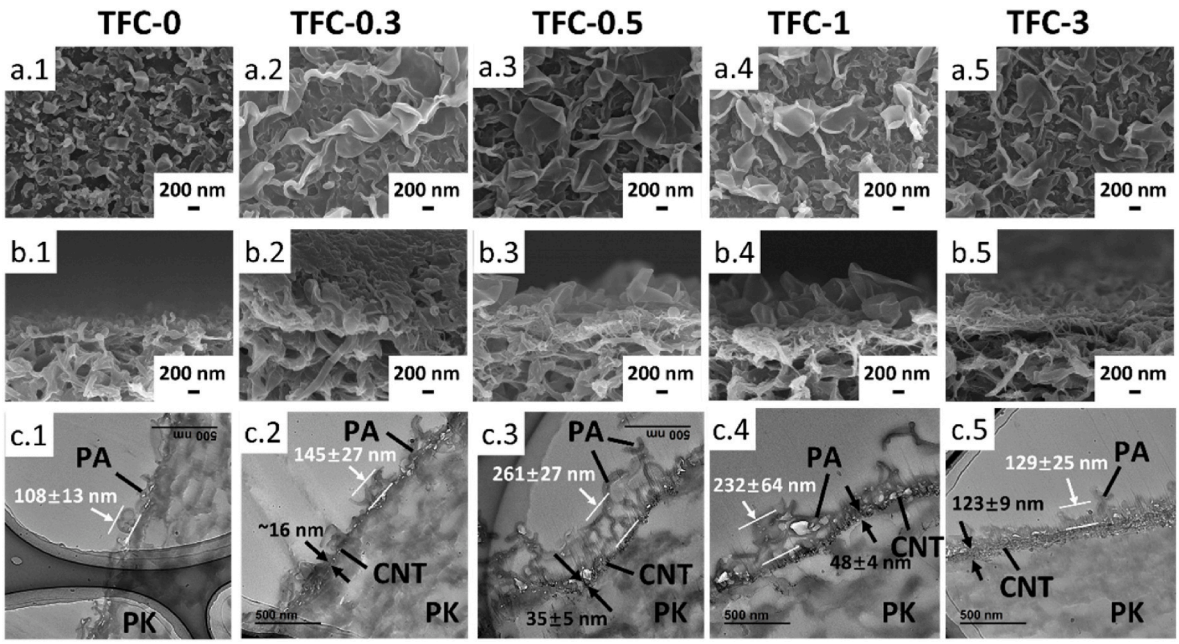

Fig. 1. (a) Surface morphology of TFC membranes imaged using FE-SEM; Cross-sectional morphology of the TFC membranes imaged using (b) field emission scanning electron microscopy (FE-SEM) and (c) transmission electron microscope (TEM). Legend: (1) Pristine TFC-0 membrane, (2–5) TFC membranes prepared with PK-CNT substrate coated with 0.3, 0.5, 1, and 3 mL of CNT dispersion, respectively (TFC-*x*, where *x* represents the volume of CNT dispersion used to coating the PK surface).

porous structure located in the lower half of the image corresponds to the PK substrate, while the crumpled structure on top represents the PA layer. Additionally, very fine fibers, identified as CNT fibers, can be seen sporadically in the CNT-interlayered samples. However, due to the interlocking structure between layers, it is challenging to distinguish the boundaries of these layers in SEM images. Therefore, TEM characterization was conducted to provide a clearer view of the layered structure of TFC membranes (Fig. 1c). In the TEM images, the PA layer, CNT intermediate layer, and PK substrate are clearly distinguishable and labeled accordingly in each image. For the PA layers, the crumpled structure becomes more pronounced after introducing CNT intermediate layer (Fig. 1c.1–3). This phenomenon was observed from the morphological images of the membranes whose intermediate layers were prepared with CNT dispersion volumes lower than 1 mL. The membranes whose intermediate layers were prepared using higher CNT dispersion amounts (TFC-1 and TFC-3) showed a reduction in leaf-like structures and another emergence of nodular structures (Fig. 1c.4–5). To further quantify the changes, we measured the thickness of the CNT layer and the apparent thickness of the crumpled PA layer based on TEM images. The average thickness of the PA layer for TFC-0 was 108 ± 13 nm. After introducing the CNT intermediate layer, the PA thickness increased to 261 ± 27 nm for TFC-0.5, then slightly decreased to 232 ± 67 nm for TFC-1. However, excessive CNT loading led to a reduction in PA thickness, measuring 129 ± 25 nm for TFC-3. This transition in the PA structure was also corroborated by the cross-sectional SEM images (Fig. 1b and **c**) and the surface roughness data listed in Table S2.

In our earlier work, we studied in detail the mechanism of these PA structural phenomena [35] which was a consequence of different IP reaction extent affected by the CNT intermediate layer. Briefly, the loading of CNT in the intermediate layer is positively correlated with the diffusion rate of the IP monomer MPD. Higher CNT loading (a thicker CNT intermediate layer) promotes MPD diffusion, which in turn facilitates the IP reaction and results in a PA layer with greater apparent thickness. However, excessive CNT loading can have the opposite effect, weakening MPD diffusion and leading to a reduction in leaf-like structures and apparent thickness of PA layer, as seen in TFC-3 [35].

3.2. GIWAXS analysis of the composite cross-linking structure of CNT-ITFN membrane

As the IP reaction happened on the surface of CNT, the CNT layer is more likely working as a bottom scaffold for the PA generation in a perpendicular direction, forming an uneven distribution of the composite structure inside the PA layer. To further demonstrate this composite structure change brought about by CNT, an investigation employing 2D grazing-incidence wide-angle X-ray scattering (GIWAXS) was conducted to elucidate the significance of intercalating CNT within the PA layer and its effect on molecular packing.

Fig. 2a–**d** shows the 2D GIWAXS patterns of TFC membranes. For all TFC membranes, scattering rings were found to be distributed across all azimuthal directions from q_z to q_{xy} (where q_z and q_{xy} denote the orientation direction of out-of-plane and in-plane, respectively), which means there are crystalline structures in the sample, however, these crystal units are randomly orientated. These ring scattering patterns are different from literatures which reported arc scattering patterns for IP-made aromatic PA film [44,45]. It should be noted that despite the quite low incident angle (0.05°) of X-ray in GIWAXS measurements (testing details are provided in the Supporting Information), the PK substrate and CNT intermediate layer can still be detected [46]. Therefore, the unusual scattering pattern of PA could be attributed to the scattering of the underlying PK substrate or CNT intermediate layer which are randomly stacking in the TFC membrane.

Upon the introduction of CNT intermediate layer between PK substrate and PA layer, two thin scattering rings gradually appeared in the patterns of TFC-0.3 and TFC-0.5 (Fig. 2b and **c**). The disappearance of ring at q_z ~2 $Å^{-1}$ could be attributed to the undetectability of PK when the much rougher PA formed on a thickened CNT scaffold (See Table S2 for surface roughness change of TFC membranes). On the other hand, the disorderly stacking of the CNT scaffold at the bottom of PA layer was detected and found to contribute to the two thin scattering rings which represent the crystalline phases CNT. Clearer boundary was found for TFC-0.5 case, as more CNT was incorporated. However, the thin double rings disappeared in the pattern of TFC-1 and replaced by a local sparking arc at q_z direction (black dashed rectangle in Fig. 2d). This

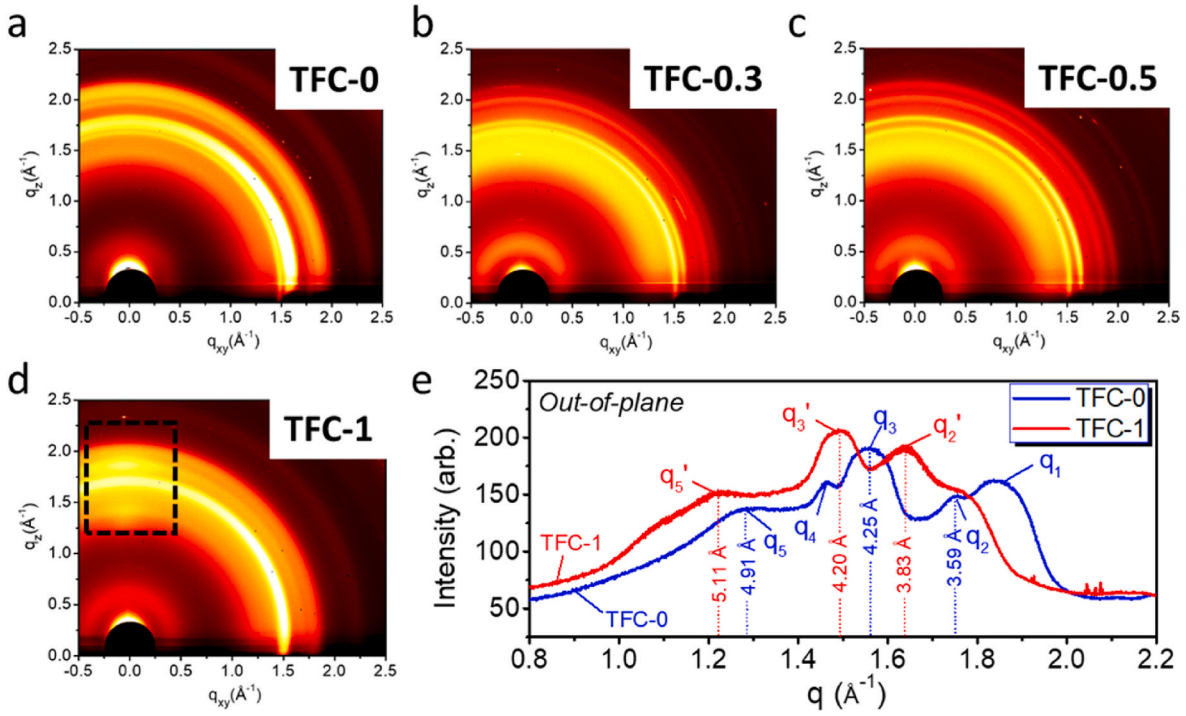

Fig. 2. 2D GIWAXS patterns of the pristine TFC-0 membrane (a) and the CNT-ITFN membranes with CNT loading of 0.3 (b), 0.5 (c) and 1 (d); Integration plots of TFC-0 and TFC-1 in the direction of out-of-plane (e). The d-spacing was calculated based on the equation of $d = (2\pi)/q$.

distinct behavior illustrates that the CNT stacking changed from uniform stacking arrangements to out-of-plane multilayer stacking, after forming a sufficient CNT network at a CNT loading of 0.5 (Fig. S1c).

Moreover, a detailed comparison of TFC-0 and TFC-1 was conducted using integration plots in an out-of-plane direction (Fig. 2e). TFC-0 shows three characteristic peaks of aromatic PA at $q_2 = 1.75$ Å^{-1}, $q_3 = 1.56$ Å^{-1} and $q_5 = 1.28$ Å^{-1}, corresponding to the π -π stacking (q_2 and q_3) and the "T-shaped" configuration (q_5) of the aromatic rings in the PA molecular chain according to reported works [44,46]. Another two peaks at $q_1 = 1.84$ Å^{-1} and $q_4 = 1.48$ Å^{-1} disappeared after introducing CNT intermediate layer (see TFC-1 profile), likely due to the increased thickness of the PA layer and CNT layer making the PK substrate undetectable, as evidenced by the 2D scattering pattern. Another significant difference for TFC-1 is the shift of the characteristic PA peaks to smaller q values: $q_2' = 1.64$ Å^{-1}, $q_3' = 1.50$ Å^{-1}, and $q_5' = 1.23$ Å^{-1}. This peak shift indicates a change in the aromatic ring motifs in the TFC-1 membrane.

The *d-spacing*, considered as the footprint to differentiate the arrangement of molecule chains in TFC membranes, was calculated according to the magnitude of scattering vector q and Bragg's law [44,47] ($d = \frac{2\pi}{q}$, the detailed calculation method is shown in Supporting Information). Considering the inversely proportional relationship between q and d, a small q indicates a larger *d-spacing* of packing motifs. The calculated *d-spacing* based on the three characteristic peaks shown in TFC-0 and TFC-1 profile are labeled in Fig. 2e. It can be observed that TFC-1 projects larger *d-spacing*s of 3.83 Å and 4.20 Å for π-π stacking, and 5.11 Å for the T-shaped configuration. Moreover, the intensity of these three shifted peaks also increased, indicating more oriented motifs formed. The large *d-spacing* and more oriented motifs detected can be attributed to the following reasons: First, the CNT scaffolds aid in rearranging the PA chains in the out-of-plane direction with controlled heterogeneity, resulting in a more permeable PA structure than TFC-0 [46], particularly when optimal CNT loading and PA cross-linking conditions are met. This promoting effect of CNT on polymer crystallization or crystal form change has also been demonstrated in other CNT-polymer blending works, although the polymers and species of CNT studied were different [48–50]. Another reason for the large *d-spacing* of TFC-1 may be signal interference from the underlying CNT scaffolds, where the large benzene ring stacking between nanotubes can be detected. Nevertheless, the T-shaped configuration exclusive to aromatic PA confirmed the increased *d-spacing* of PA for TFC-1, which is preferential for water diffusion [46]. These findings contribute to a more comprehensive understanding of the composite structure within CNT-ITFN membranes.

On the other hand, there are few studies on the structure of TFC membranes using GIWAXS. Most have characterized the single PA layer by dissolving the substrate with solvents to diminish substrate influence. However, solvent treatment could also cause changes in the PA crystalline structure, affecting the results. Our work is the first attempt to apply GIWAXS technology, a method mainly used for structural characterization of conjugated polymers [51,52], to study this CNT-ITFN membrane *in situ*, demonstrating a potential method for other TFC membranes. In the future, more research on the substrate structure or the incident angle of X-ray (e.g., detecting depth) is worth conducting to provide more detailed information for the composite structure of TFC membranes.

3.3. Influence of CNT intermediate layer on surface charge of TFC membrane

In an earlier work, the CNT intermediate layer was proved to influence the IP reaction by promoting the monomer release, resulting in different extents of IP reaction which could bring a difference on the charge property of PA layer [35]. To illustrate this potential change on surface charge, we first measured the zeta potential of the pristine and the CNT-ITFN membranes over a pH range of 3–10. Comparing the CNT-ITFN membranes, there was a clear change in the surface zeta potential as the CNT dispersion coating volume increased. As shown in Fig. 3a, with an increase of CNT dispersion coating volume from 0.1 mL to 1 mL, the surface of TFC membrane became less negative, with TFC-1 membrane exhibiting generally neutral to positive charges at all pH values. Further increasing the CNT dispersion volume did not result in

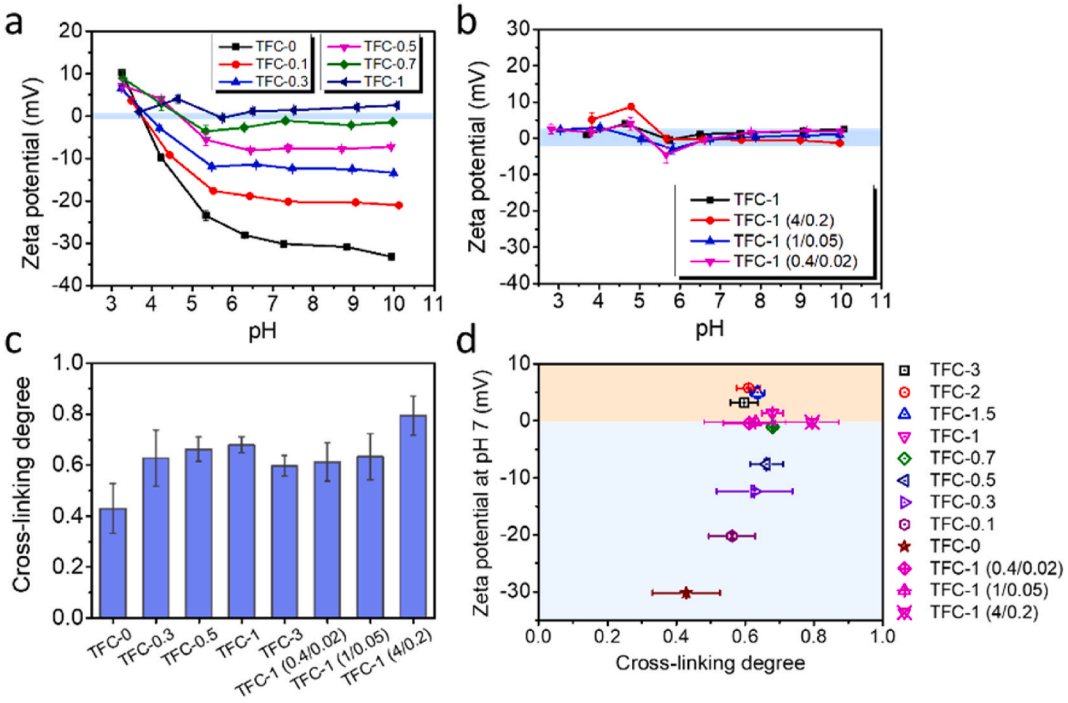

Fig. 3. (a) Zeta potential of TFC membranes having different CNT loading amount (TFC-*x*, where *x* represents the volume of CNT dispersion used to coating the PK surface; the IP monomer concentrations were fixed at 2 wt% MPD and 0.1 wt% TMC); (b) Zeta potential of the TFC membranes fabricated using different MPD and TMC concentration under a fixed CNT coating volume of 1 mL (TFC-1 (*x*/*y*), where the *x* and y represent the weight percent of MPD and TMC); (c) Calculated cross-linking degree (Numerical data was provided in Table S3); (d) Correlation of the zeta potential and the cross-linking degree of TFC membranes prepared in this work.

any significant change in the membrane surface zeta potential.

To further demonstrate the changes on surface charge, the CNT-ITFN membranes prepared using different IP monomer concentrations: (1) 0.4 wt% MPD and 0.02 wt% TMC; (2) 1 wt% MPD and 0.05 wt% TMC; (3) 4 wt% MPD and 0.2 wt% TMC, under a fixed CNT loading at 1, were characterized for zeta potential measurements and surface morphology. The surface morphologies of these TFC membranes were shown in Fig. S3. Despite the differences in the PA morphology and the MPD and TMC monomer concentrations during the IP process, the neutral property was still found on these TFC membranes, as shown in Fig. 3b. It is widely known that the negative surface charge of PA layer is mainly attributed to the carboxyl groups hydrolyzed from the unreacted acyl chloride groups of TMC. The less negative charges mean the less carboxyl groups remained on the PA surface, which means less acyl chloride groups were hydrolyzed, indicating that more acyl chloride groups had reacted with the amine groups of MPD during the IP reaction, leading to a higher PA cross-linking degree.

Based on this, we calculated the cross-linking degree of PA according to the X-ray photoelectron spectroscopy (XPS) analysis (Fig. S4). The cross-linking degree of PA selective layers were shown in Fig. 3c. The pristine TFC membrane has a cross-linking degree of 0.43, and it was observed to increase with the intercalation of the CNT intermediate layer. This indicates that the introduction of nano-sized materials and intermediate layer could influence polyamide formation [53,54]. As the CNT loading increased, the cross-linking degree was observed to increase as well, with the highest cross-linking degree of 0.68 for TFC-1 (TFC membrane prepared using PK substrate coated with 1 mL CNT dispersion). Further increasing the amount of CNT coating on the membrane substrate resulted in a slightly lower cross-linking degree value of 0.60 for TFC-3 membrane, which were still higher than that of the pristine TFC membrane. The cross-linking degree of the TFC-1 (0.4/0.02), TFC-1 (1/0.05), and TFC-1 (2/0.1) were also determined, and all showed similar cross-linking degrees of 0.61–0.68. Comparing these three, there was a noticeable increase as the amount of IP monomers, but the changes were only marginal. TFC-1 (4/0.2), on the other hand, exhibited the highest cross-linking degree of 0.79, which could be attributed to the facilitation of more PA formation when there were more reactants present during the reaction.

Earlier studies have reported that the cross-linking during IP could influence the surface charge of TFC membrane. Therefore, we correlated the cross-linking degree with the zeta potential values at pH 7. It is observed that there was a clear correlation between the membranes' cross-linking degree and their charge densities (Fig. 3d). The pristine TFC membrane (TFC-0) was observed to have the lowest cross-linking and the most negatively charged membrane surface, as well. When the CNT intermediate layer was introduced, there was an observed increase in cross-linking degree and decrease in negative surface charge, but only until the TFC membranes prepared with PK substrate coated with 1 mL CNT dispersion (TFC-1, TFC-1 (0.4/0.02), TFC-1 (1/0.05), and TFC -1 (4/0.2)). For the membranes prepared with higher CNT coating amounts, slightly lower cross-linking degrees were observed but the surface zeta potential of the membranes were all observed to be positive. These results demonstrate well the positive correlation between cross-linking degree and surface charge property on condition of a CNT-regulated IP reaction which has been investigated and elucidated in our earlier work [35]. To be specific, the CNT coating on the PK membrane substrate facilitated the MPD monomer release due to the hydrophobic nature of CNT and the smaller pore size of CNT network. The pristine PK substrate, endowed with large surface porosity and excellent hydrophilicity, allows easy penetration of MPD, leading to a high MPD storage capacity; however, the interaction between the PK and MPD retards the release of MPD to react with TMC [55]. On the other hand, the presence of the hydrophobic CNT intermediate layer results in a reduced but sufficient MPD supply and an increased MPD release rate. The heightened MPD release rate could allow more interaction between MPD and TMC, resulting in higher cross-linking degree and less presence of hydrolyzable carboxyl groups, effectively lowering the negative surface charge of the membrane.

Earlier studies, which involved amine grafting on top of TFC membranes and secondary IP, attributed the generally less negative charges

of TFC membranes to the consumption of the carboxyl (COO−) groups during the reaction with amine groups that occurred during the grafting and successive IP processes [23,41,42]. However, in the case of this work, no further modification was conducted on the PA layer, except for the intercalation of CNT intermediate layer, which introduces a novel way to tailor the surface charge of TFC membranes.

3.4. Reverse osmosis performance of CNT-ITFN membrane

The performance of the pristine and the CNT-ITFN membranes were tested in RO process. Fig. 4 shows the pure water permeability (*A*) and NaCl rejection of the TFC membranes. All the CNT-ITFN membranes exhibited increased water permeability, in comparison with the pristine TFC membrane (TFC-0). The TFC-0 membrane demonstrated pure water permeability of 1.31 L m^{-2} h^{-1}/bar, and as an effect of the intercalation of CNT intermediate layer, the *A* value became 1.60 (TFC-0.5), 2.43 (TFC-1), 1.56 (TFC-3) L m^{-2} h^{-1}/bar without NaCl rejection loss (Fig. 4a). The increase in permeability is mainly attributed to the role of the CNT intermediate layer as a gutter layer, which shortens the transport distance within the PA selective layer. Specifically, water molecules can transport along the porous CNT network once they pass through the PA layer in a vertical path. This effectively shortens the transport distance within the low-permeable PA layer. In contrast, for the TFC membrane without CNT intermediate layer (TFC-0), water molecules must transport transversely inside the PA until they reach the pore domain of the substrate, leading to lower permeance. Moreover, a suitable CNT intermediate layer provides a favorable platform for PA generation, effectively reducing the growth of PA into the macropores of the substate [39,40]. Less PA intrusion means less transport resistance, which is beneficial for high permeance. However, the higher CNT coating thickness of TFC-3 membrane also resulted in increased transport resistance, which retarded water permeability [37]. Additionally, the CNT-ITFN membranes have a rougher PA surface with higher apparent thickness, ensuring a larger area for transport and thereby improving permeability [56]. It is worth noting that this permeability improvement is the result of multiple factors, requiring an appropriate amount of CNT coating to maximize this enhancement, as seen with TFC-1 in this case. Too little or too much CNT coating can compromise one of the benefits, resulting in less impressive results. For example, too little CNT coating may not effectively prevent the growth of PA inside the substrate, leading to a lesser extent of reduced transport resistance.

An application of neutral- or positively-charged membranes is their ability to retain and concentrate NH_4^+ in solution [23,41]. It was previously established that, for NH_4^+ rejection and concentration, the surface charge and cross-linking degree of the membrane could play a crucial role. Specifically, a neutral- or positively-charged TFC membrane with less unreacted carboxyl groups can be more effective at rejecting NH_4^+ compared to the conventionally negatively charged pristine TFC membrane [23]. Thus, the NH_4^+ rejection performance of TFC membranes was evaluated by using 400 mg L^{-1} NH_4^+ from NH_4Cl as feed solution, and results were shown in Fig. 4b. The NH_4^+ rejection increased from 90.7 % for TFC-0 to 95.2 % for TFC-1 and 96.0 % for TFC-3, with TFC-1 having the highest permeance. The increased NH_4^+ rejection can be attributed to the higher degree of cross-linking and the neutral surface property of TFC-1. Normally, NH_4^+ shares a similar hydraulic radius with water molecules [57]. An increased degree of cross-linking helps the TFC-1 membrane discriminate between these two, further enhancing NH_4^+ removal. Additionally, electrostatic interactions exist between the membrane surface and NH_4^+. A negatively charged membrane surface tends to have more interactions with NH_4^+, leading to a compromised NH_4^+ rejection [41,58,59]. Considering this, the TFC-1 membrane in this work exhibits not only the highest degree of cross-linking but also a neutral surface property, which reduces electrostatic interactions. These two benefits together ensure enhanced NH_4^+ rejection compared with the negatively charged TFC-0 and TFC-0.5 membranes. For the neutral TFC-3 membrane, the reduced electrostatic interaction was more dominant, allowing it to maintain high NH_4^+ rejection despite a slightly decreased cross-linking degree.

Regulation of the membrane surface charge has also been found as a useful method to improve the fouling resistance of membranes [22]. Previously, development of fouling-resistant membranes mainly focused on the surface hydrophilization [60–63]; however, fouling is also regulated by other factors aside from the membrane surface hydrophilicity, such as surface charge and roughness. Generally, higher hydrophilicity and lower surface roughness are favorable for fouling resistance due to the thicker hydration layer formed on the surface and the easier removal of foulants from the surface [64–67]. However, in this work, all CNT-ITFN membranes have rougher and more hydrophobic surface features than the pristine TFC-0 membrane due to the enhanced IP reaction brought about by the CNT intermediate layer (Fig. 1 and Table S2). In this case, it is more reasonable to discuss the antifouling performance from the perspective of charge effect. Moreover, to provide a clear evaluation of the antifouling performance, the fouling propensity of the TFC membranes prepared in this work was tested in both static adsorption and dynamic filtration methods.

Considering that the surface of TFC membrane is initially negatively charged, lysozyme (LYZ), a positively charged model protein foulant, was first used to demonstrate the fouling resistance of the TFC membranes in a static adsorption test. Fig. 5a.1–3 show the confocal laser scanning microscope (CLSM) images of the TFC-0, TFC-0.5, and TFC-1 membrane, respectively, after immersion in a phosphate buffered saline (PBS) solution (pH 7.4) containing 20 mg L^{-1} fluorescent LYZ (FTIC LYZ). At pH 7.4, LYZ is positively charged, thus it was somehow expected that the pristine TFC-0 membrane suffered from the highest attachment of the fluorescent protein, compared with TFC-0.5 and TFC-1. The lower FTIC LYZ attachment on both TFC-0.5 (0.56 a.u.) and TFC-1 (0.30 a.u.) compared to TFC-0 (4.98 a.u.) could be attributed to the less negative membrane surface charge (Fig. 5c), resulting in weaker

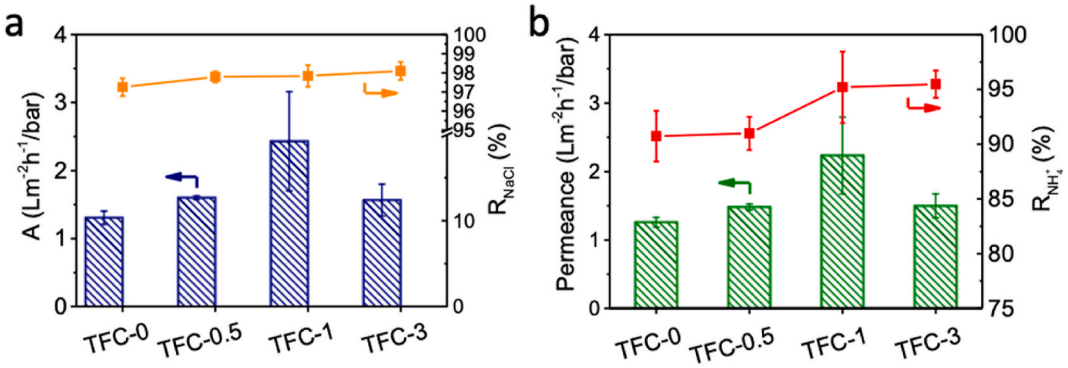

Fig. 4. Reverse osmosis filtration performance of TFC membranes. (a) Pure water permeability (*A*) and NaCl rejection (R_{NaCl}) determined using deionized water and 2000 mg L^{-1} NaCl as feed solutions, respectively; (b) Permeance and NH_4^+ rejection (R_{NH4+}) determined using 400 mg L^{-1} NH_4^+ from NH_4Cl as feed solution.

electrostatic attraction between the membrane surface and the positively charged protein. Similar static adsorption behavior was observed for *E. coli*. Fig. 5b.1–3 show the CLSM images of the membranes after incubation in *E. coli*, and the corresponding fluorescent intensity values are shown in Fig. 5c. Due to the negative charge of the pristine TFC membrane, there was electrostatic repulsion with the bacteria, resulting in very low bacterial attachment (0.15 a.u.). Similarly, the less negative TFC-0.5 (0.26 a.u.) and the neutral charged TFC-1 membranes (0.13 a.u.) hardly showed any bacterial adhesion. The surface charge of the TFC-1 membrane is close to zero, thus there was no electrostatic attraction between the membrane and the charge-bearing *E. coli*.

From the above results, it is evident that the neutral TFC-1 membrane exhibits better anti-adsorption performance against both positively charged protein and negatively charged bacteria. This is mainly attributed to its neutral surface property, which weakens the electrostatic effect [67]. Certainly, surface hydrophilicity and surface roughness are also important factors influencing the adsorption behavior through hydrophobic interactions and interlocking structures [68]. However, the relatively minor differences in hydrophilicity among all TFC membranes and the increased surface roughness for CNT-ITFN membranes suggest that the charge effect predominates in anti-adsorption performance.

Dynamic fouling filtrations were performed in this study by using two positive-charged organic model foulants, LYZ and surfactant cetyltrimethylammonium bromide (CTAB), to provide confirmation of the fouling control of neutral TFC membranes. The data shown in Fig. 6a and **b** corresponds to the filtration results using feed solutions containing 200 mg L^{-1} of LYZ and CTAB, respectively. In Fig. 6a, there was no discernible difference in the filtration performances of TFC-0 and TFC-1 membrane. Both membranes experienced flux decline of around 20 % until the end of the operation. This was different from the results of the static protein foulant adsorption results discussed earlier (Fig. 5a). This could be attributed to the increased surface roughness of TFC-1 (Table S2). Unlike static absorption, in dynamic fouling tests, surface roughness significantly affects foulant deposition by creating interlocking structures. Foulants can easily become trapped in the micro-nanostructures on the membrane surface and are difficult to detach under hydraulic forces, leading to extensive foulants deposition [69]. It is precisely because of the effect of roughness on dynamic fouling that the advantage of TFC-1's neutral property in antifouling was diminished.

Another commonly used organic model foulant, the positively charged surfactant CTAB, was used to further evaluate the antifouling performance of TFC membranes. The dynamic filtration results over two filtration cycles are shown in Fig. 6b. Unlike the LYZ fouling profile, the

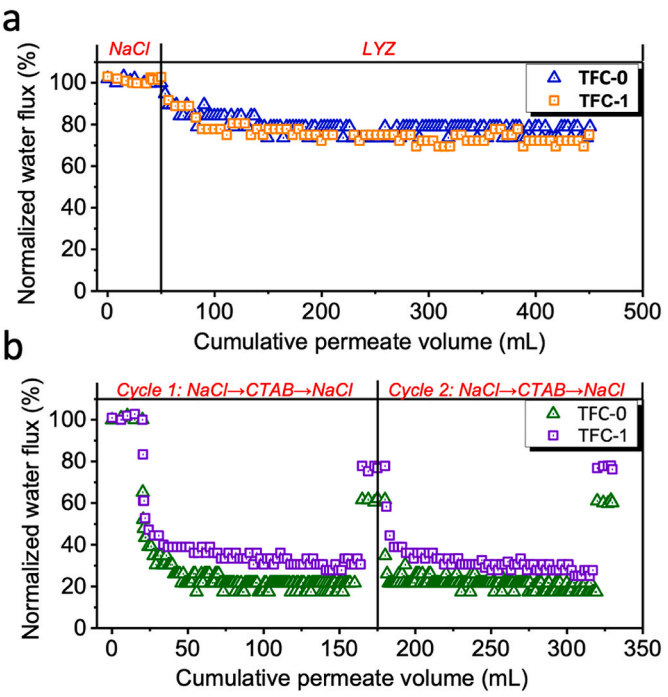

Fig. 6. Dynamic filtration results of TFC-0 and TFC-1 membrane using model foulants (a) LYZ and (b) CTAB. 200 mg L^{-1} model foulants in 2000 mg L^{-1} NaCl were used as the feed solutions. (Complete filtration protocol was provided in the Supporting Information.)

distinct flux pattern induced by CTAB showed a faster flux decline compared to LYZ. This severe fouling pattern from the positively charged surfactant is consistent with previous findings [70,71]. Due to the small molecular weight of CTAB (364.5 g/mol), a higher number of CTAB molecules approach the membrane surface compared to LYZ, especially at an identical concentration of 200 mg L^{-1}, resulting in overall more severe fouling by CTAB than LYZ. In the first fouling cycle, the TFC-1 membrane showed better antifouling performance than TFC-0, evidenced by a lower flux decline (30 % of initial flux remaining for TFC-1 compared to 20 % of TFC-0). After replacing the CTAB feed solution with NaCl solution, the flux of the TFC-1 membrane recovered to 80 % of its initial value, while TFC-0 only recovered to 60 %. Similar performance was observed during the second filtration cycle (Fig. 6b). The lower flux decline and higher flux recovery demonstrate that the neutral TFC-1 membrane exhibits better antifouling properties than

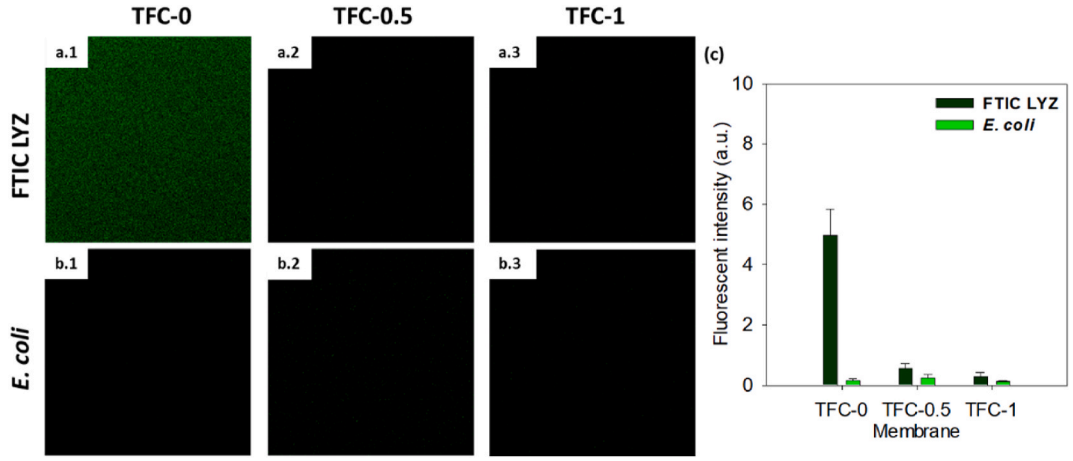

Fig. 5. CLSM images of TFC membranes after incubation in (a) FTIC LYZ and (b) *E. coli*; (c) Fluorescent intensity values calculated using ImageJ software. Legend: (1) Pristine TFC-0 membrane, (2 and 3) CNT-ITFN membranes prepared with PK-CNT substrates coated with 0.5 and 1 mL of CNT dispersion.

TFC-0. For the negatively charged TFC-0 membrane, strong attractive electrostatic interactions with positively charged molecules like CTAB lead to severe flux decline [72]. In contrast, TFC-1's neutral surface property reduces these electrostatic interactions [72], resulting in reduced flux decline. Moreover, weaker electrostatic attraction also facilitates foulant detachment during cleaning, contributing to higher flux recovery for TFC-1.

It is noteworthy that the difference in antifouling properties between the two membranes is not significant, whether for proteins or surfactants. This might be attributed to the increased surface roughness of TFC-1, which is not an ideal feature for resisting foulant attachment and somewhat offsets the benefits of a neutral surface, as discussed earlier. Nonetheless, this study highlights a promising approach to adjust the surface charge of TFC membranes using CNT intermediate layer to potentially enhance antifouling properties, provided that good hydrophilicity and low surface roughness are maintained.

3.5. Comparison with other methods for surface charge tailoring

Comparing different methods for regulating surface charge in terms of membrane antifouling performance is challenging due to the strong dependence of membrane fouling on various conditions such as ion species and concentration, filtration operating time, and cleaning methods for flux recovery measurements (Table S4). We have summarized a table listing several representative charge tailoring methods along with their membrane performances in NH_4^+ rejection and antifouling performance in Table S4. It is evident that our neutral CNT-ITFN membrane (TFC-1) did not dominate in terms of fouling resistance compared to reported works. The variability in fouling conditions across studies, even with the same foulant, complicates the assessment of the modification method effectiveness based solely on fouling data. One contributing factor to the less remarkable results is the high roughness and hydrophobicity of TFC-1, which compromise the benefits of its neutral charge property on antifouling, as discussed earlier. This resulted in minimal differences compared to the pristine membrane sample (TFC-0). However, setting fouling data aside, our membrane maintains an advantage in maintaining a neutral charge across a wider pH range, unlike other membranes that only exhibited zero charge under specific pH conditions. This property is crucial as the pH of feed solution can influence the isoelectric point of foulants, especially proteins [73]. Regarding NH_4^+ rejection, our membrane demonstrates comparable performance in NH_4^+ rejection and water permeance to commercial seawater RO membranes, which are highly dense. Additionally, our membrane shows antifouling properties due to its neutral surface characteristics, whereas commercial RO membranes are susceptible to fouling during filtration.

Among the charge regulation methods listed in Table S4, surface modification is the most used approach. This method involves grafting neutral molecules onto the surface or introducing chemical groups with opposite charges to neutralize the original charge on the surface. For TFC membranes, the unreacted acyl chloride groups or carboxyl groups hydrolyzed from acyl chloride usually serve as grafting anchors [74]. This method offers the advantage of affecting other properties such as hydrophilicity to achieve a synergistic effect on fouling resistance and separation. However, this strategy requires modification after the IP reaction, and the chemical treatment could potentially damage the PA layer, compromising salt rejection. Moreover, achieving zero charge over a wider pH range may be challenging with this method, limiting its applicability in diverse solvent environments. In contrast, our strategy involves regulating the surface charge of the PA selective layer simply by intercalating a CNT intermediate layer before the IP reaction. This approach maintains a neutral surface property across a wider pH range, which is a distinct advantage that other methods may not achieve. Nevertheless, other membrane properties must always be considered for specific applications, such as fouling mitigation, as demonstrated in this study. Overall, this work introduces an effective method for tailoring the surface charge of PA selective layers of TFC membrane, providing novel insights for researchers involved in membrane surface engineering. While the reduction of PA membrane surface negative charge following CNT intermediate layer intercalation via inkjet printing prior to the IP reaction of piperazine and TMC has earlier been observed [75], the mechanism behind the phenomenon was not fully elucidated and the implications of the surface charge regulation were not investigated. Following the findings resulting from this work, future research in this area should focus on deepening the understanding of the mechanisms and applications of the neutral CNT-ITFN membrane, including applying the CNT intermediate layer to TFC membranes with originally low surface roughness and good hydrophilicity.

4. Conclusion

In this work, CNTs were coated on the top of PK membrane substrates prior to PA selective layer formation via IP reaction. The presence of CNT intermediate layer brought about changes in PA morphology and chemical structure. Lower CNT coating amounts facilitated the large leaf-like structure formation of PA by increasing the MPD release rate during IP. Excessive CNT loading could weaken this facilitation as a drawback of PA structure was observed. The 2D GIWAXS measurement was firstly used to characterize the composite structure of PA layer. The CNT scaffolds were confirmed aid in the rearrangement of the PA chains with a controlled heterogeneity to have a larger *d-spacing*. The chemical composition analysis confirmed an increased cross-linking degree of PA upon increasing the CNT loading, until at a maximum value obtained for TFC-1. Interestingly, a positive correlation was drawn between the cross-linking degree and the membrane surface charge, with TFC-1 having a neutral property regardless of the IP concentration. This CNT-dependent regulation offers a novel way to regulate the surface charge of TFC membrane.

In the performance, due to the gutter layer effect of CNT and large filtration of PA and its neutral surface property, the TFC-1 membrane exhibited enhanced desalination and NH_4^+ rejecting performance in RO process. The static adhesion and dynamic filtration measurements showed that the TFC-1 membrane had less attachment of model foulants LYZ and *E. coli*, and exhibited lower flux decline ratio and higher flux recover ratio during the dynamic filtration tests. The better antifouling performances of TFC-1 demonstrated the advantage of neutral surface property in reducing electrostatic attractions between foulants and surfaces. However, this benefit can be offset by the other surface properties such as hydrophilicity and roughness, as less significant differences were observed from the antifouling results.

CRediT authorship contribution statement

Luyao Deng: Writing – review & editing, Writing – original draft, Visualization, Methodology, Investigation, Formal analysis, Data curation, Conceptualization. **Ralph Rolly Gonzales:** Writing – review & editing, Writing – original draft, Visualization, Supervision, Methodology, Formal analysis, Data curation, Conceptualization. **Joy Thomas:** Writing – original draft, Investigation, Formal analysis. **Ryosuke Takagi:** Writing – review & editing, Investigation. **Wenming Fu:** Investigation. **Cheng-Liang Liu:** Investigation. **Shang Xiang:** Investigation. **Hideto Matsuyama:** Writing – review & editing, Supervision, Resources, Project administration.

Declaration of competing interest

The authors declare that they have no known competing financial interests or personal relationships that could have appeared to influence the work reported in this paper.

Acknowledgment

This work is part of a project (Project Number: JPNP18016) commissioned by the New Energy and Industrial Technology Development Organization (NEDO), Japan. Luyao Deng acknowledge the China Scholarship Council (CSC) for financial support (No. 202208050066) during her PhD study.

Appendix A. Supplementary data

Supplementary data to this article can be found online at https://doi.org/10.1016/j.compositesb.2024.111951.

Data availability

Data will be made available on request.

References

[1] Shannon MA, Bohn PW, Elimelech M, Georgiadis JG, Mariñas BJ, Mayes AM. Science and technology for water purification in the coming decades. Nature 2008;452(7185):301–10.
[2] Volpin F, Gonzales RR, Lim S, Pathak N, Phuntsho S, Shon HK. GreenPRO: a novel fertiliser-driven osmotic power generation process for fertigation. Desalination 2018;447:158–66.
[3] Gude VG. Desalination and water reuse to address global water scarcity. Rev Environ Sci Biotechnol 2017;16(4):591–609.
[4] van Vliet MTH, Jones ER, Flörke M, Franssen WHP, Hanasaki N, Wada Y, et al. Global water scarcity including surface water quality and expansions of clean water technologies. Environ Res Lett 2021;16(2):024020.
[5] Chung T-S, Zhao D, Gao J, Lu K, Wan C, Weber M, et al. Emerging R&D on membranes and systems for water reuse and desalination. Chin J Chem Eng 2019;27(7):1578–85.
[6] Nicolaisen B. Developments in membrane technology for water treatment. Desalination 2003;153(1):355–60.
[7] Quist-Jensen CA, Macedonio F, Drioli E. Membrane technology for water production in agriculture: desalination and wastewater reuse. Desalination 2015;364:17–32.
[8] Wenten IG. Khoiruddin. Reverse osmosis applications: prospect and challenges. Desalination 2016;391:112–25.
[9] Lau WJ, Ismail AF, Misdan N, Kassim MA. A recent progress in thin film composite membrane: a review. Desalination 2012;287:190–9.
[10] Jegal J, Min SG, Lee K-H. Factors affecting the interfacial polymerization of polyamide active layers for the formation of polyamide composite membranes. J Appl Polym Sci 2002;86(11):2781–7.
[11] Kong C, Shintani T, Kamada T, Freger V, Tsuru T. Co-solvent-mediated synthesis of thin polyamide membranes. J Membr Sci 2011;384(1–2):10–6.
[12] Qiu S, Wu L, Zhang L, Chen H, Gao C. Preparation of reverse osmosis composite membrane with high flux by interfacial polymerization of MPD and TMC. J Appl Polym Sci 2009;112(4):2066–72.
[13] Ismail AF, Padaki M, Hilal N, Matsuura T, Lau WJ. Thin film composite membrane — recent development and future potential. Desalination 2015;356:140–8.
[14] Hailemariam RH, Woo YC, Damtie MM, Kim BC, Park K-D, Choi J-S. Reverse osmosis membrane fabrication and modification technologies and future trends: a review. Adv Colloid Interface Sci 2020;276:102100.
[15] Ji C, Zhai Z, Jiang C, Hu P, Zhao S, Xue S, et al. Recent advances in high-performance TFC membranes: a review of the functional interlayers. Desalination 2021;500:114869.
[16] Ankoliya D, Mehta B, Raval H. Advances in surface modification techniques of reverse osmosis membrane over the years. Separ Sci Technol 2018;54(3):293–310.
[17] Zhang Z, Kang G, Yu H, Jin Y, Cao Y. From reverse osmosis to nanofiltration: precise control of the pore size and charge of polyamide membranes via interfacial polymerization. Desalination 2019;466:16–23.
[18] Reis R, Duke M, Merenda A, Winther-Jensen B, Puskar L, Tobin MJ, et al. Customizing the surface charge of thin-film composite membranes by surface plasma thin film polymerization. J Membr Sci 2017;537:1–10.
[19] Ishigami T, Amano K, Fujii A, Ohmukai Y, Kamio E, Maruyama T, et al. Fouling reduction of reverse osmosis membrane by surface modification via layer-by-layer assembly. Separation and Purification Technology 2012;99:1–7.
[20] Zhu X, Jańczewski D, Guo S, Lee SSC, Parra Velandia FJ, Teo SL-M, et al. Polyion multilayers with precise surface charge control for antifouling. ACS Appl Mater Interfaces 2015;7(1):852–61.
[21] Wang Y, Wang Q, Xia Q-C, Yang W-J, Wang X-X, Sun S-P, et al. Nanocapsule controlled interfacial polymerization finely tunes membrane surface charge for precise molecular sieving. Chem Eng J 2021;409:128198.
[22] Wang S-Y, Gonzales RR, Zhang P, Istirokhatun T, Takagi R, Motoyama A, et al. Surface charge control of poly(methyl methacrylate-co-dimethyl aminoethyl methacrylate)-based membrane for improved fouling resistance. Separation and Purification Technology 2021;279:119778.
[23] Li J, Gonzales RR, Takagi R, Yao X, Zhang P, Istirokhatun T, et al. Surface modification of thin film composite forward osmosis membrane using tris(2-aminoethyl)amine for enhanced ammonium recovery. Desalination 2022;541:116002.
[24] Yin Y, Zhao Y, Li C, Wang R. Fabrication of polyamide hollow fiber nanofiltration membrane with intensified positive surface charge density via a secondary interfacial polymerization. J Membr Sci 2023;682:121778.
[25] Werber JR, Bull SK, Elimelech M. Acyl-chloride quenching following interfacial polymerization to modulate the water permeability, selectivity, and surface charge of desalination membranes. J Membr Sci 2017;535:357–64.
[26] Cheng X, Peng Y, Li S, Su B. Alginate hydrogel interlayer assisted interfacial polymerization for enhancing the separation performance of reverse osmosis membrane. J Membr Sci 2021;638:119680.
[27] Gohil JM, Ray P. A review on semi-aromatic polyamide TFC membranes prepared by interfacial polymerization: potential for water treatment and desalination. Separation and Purification Technology 2017;181:159–82.
[28] Jin Y, Su Z. Effects of polymerization conditions on hydrophilic groups in aromatic polyamide thin films. J Membr Sci 2009;330(1–2):175–9.
[29] Lim YJ, Goh K, Lai GS, Zhao Y, Torres J, Wang R. Unraveling the role of support membrane chemistry and pore properties on the formation of thin-film composite polyamide membranes. J Membr Sci 2021;640:119805.
[30] Kahrizi M, Gonzales RR, Kong L, Matsuyama H, Lu P, Lin J, et al. Significant roles of substrate properties in forward osmosis membrane performance: a review. Desalination 2022;528:115615.
[31] Chan W-F, Chen H-y, Surapathi A, Taylor MG, Shao X, Marand E, et al. Zwitterion functionalized carbon nanotube/polyamide nanocomposite membranes for water desalination. ACS Nano 2013;7(6):5308–19.
[32] Park JS, Park JY, Kim JS, Kang Y, Kim SM, Song KS, et al. Molecular-level network engineering of crosslinker towards high-performance carbon nanotube fiber. Compos B Eng 2024;275:111338.
[33] Mamidi N, Velasco Delgadillo RM, Barrera EV, Ramakrishna S, Annabi N. Carbonaceous nanomaterials incorporated biomaterials: the present and future of the flourishing field. Compos B Eng 2022;243:110150.
[34] Chen S, Chen Z, Ou Y, Lyu J, Li J, Liu X, et al. Flexible multiwalled carbon nanotubes/cellulose nanofibers membrane with rapid temperature increasing induced by interface strengthening. Compos Appl Sci Manuf 2024;177:107911.
[35] Deng L, Gonzales RR, Fu W, Xu G, Song Q, Takagi R, et al. Carbon nanotubes regulated polyamide membrane by intercalation to improve the organic solvent nanofiltration performance. Carbon 2024;216:118582.
[36] Yang Z, Sun P-F, Li X, Gan B, Wang L, Song X, et al. A critical review on thin-film nanocomposite membranes with interlayered structure: mechanisms, recent developments, and environmental applications. Environ Sci Technol 2020;54(24):15563–83.
[37] Long L, Wu C, Yang Z, Tang CY. Carbon nanotube interlayer enhances water permeance and antifouling performance of nanofiltration membranes: mechanisms and experimental evidence. Environ Sci Technol 2022;56(4):2656–64.
[38] Wang F, Yang Z, Tang CY. Modeling water transport in interlayered thin-film nanocomposite membranes: gutter effect vs funnel effect. ACS ES&T Engineering 2022;2(11):2023–33.
[39] Zhou ZY, Hu YX, Boo C, Liu ZY, Li JQ, Deng LY, et al. High-performance thin-film composite membrane with an ultrathin spray-coated carbon nanotube interlayer. Environ Sci Technol Lett 2018;5(5):243–8.
[40] Gong G, Wang P, Zhou Z, Hu Y. New insights into the role of an interlayer for the fabrication of highly selective and permeable thin-film composite nanofiltration membrane. ACS Appl Mater Interfaces 2019;11(7):7349–56.
[41] Yao X, Gonzales RR, Sasaki Y, Lin Y, Shen Q, Zhang P, et al. Surface modification of FO membrane for improving ammoniacal nitrogen (NH4+-N) rejection: investigating the factors influencing NH4+-N rejection. J Membr Sci 2022;650:120429.
[42] Gonzales RR, Sasaki Y, Istirokhatun T, Li J, Matsuyama H. Ammonium enrichment and recovery from synthetic and real industrial wastewater by amine-modified thin film composite forward osmosis membranes. Separation and Purification Technology 2022;297:121534.
[43] Li S, Xie T, Ma L, Li B, Liu D, Huang N, et al. Advanced bifunctional bionic neural network-like architecture constructed by multi-scale carbon nanotubes nanocomposites for enhanced microwave absorption. Compos B Eng 2024;284:111714.
[44] Fu Q, Verma N, Ma H, Medellin-Rodriguez FJ, Li R, Fukuto M, et al. Molecular structure of aromatic reverse osmosis polyamide barrier layers. ACS Macro Lett 2019;8(4):352–6.
[45] Fu Q, Verma N, Hsiao BS, Medellin-Rodriguez F, Beaucage PA, Stafford CM, et al. X-Ray scattering studies of reverse osmosis materials. Synchrotron Radiat News 2020;33(4):40–5.
[46] Wang L, Yang H, Li H, Lu P, Yu Y, Zhang X, et al. Diazotized polyamide membranes on commercial polyethylene textile with simultaneously improved water permeance, salt rejections and anti-fouling. Desalination 2023;549:116307.
[47] Rivnay J, Mannsfeld SC, Miller CE, Salleo A, Toney MF. Quantitative determination of organic semiconductor microstructure from the molecular to device scale. Chemical reviews 2012;112(10):5488–519.
[48] Phang IY, Ma J, Shen L, Liu T, Zhang WD. Crystallization and melting behavior of multi-walled carbon nanotube-reinforced nylon-6 composites. Polym Int 2005;55(1):71–9.
[49] Li J, Fang Z, Tong L, Gu A, Liu F. Polymorphism of nylon-6 in multiwalled carbon nanotubes/nylon-6 composites. J Polym Sci B Polym Phys 2006;44(10):1499–512.

[50] Brosse A-C, Tencé-Girault S, Piccione PM, Leibler L. Effect of multi-walled carbon nanotubes on the lamellae morphology of polyamide-6. Polymer 2008;49(21):4680–6.
[51] Zhang J, Zhang K, Xu F, Wang S, Qiu Y. Thermoelectric transport in ultrathin poly(3,4-ethylenedioxythiophene) nanowire assembly. Compos B Eng 2018;136:234–40.
[52] Shih W-C, Matsuda M, Konno K, Lin P-S, Higashihara T, Liu C-L. Tailored thermoelectric performance of poly(phenylene butadiynylene)s/carbon nanotubes nanocomposites towards wearable thermoelectric generator application. Compos B Eng 2024;286:111779.
[53] Gonzales RR, Zhang L, Guan K, Park MJ, Phuntsho S, Abdel-Wahab A, et al. Aliphatic polyketone-based thin film composite membrane with mussel-inspired polydopamine intermediate layer for high performance osmotic power generation. Desalination 2021;516:115222.
[54] Lai GS, Lau WJ, Goh PS, Karaman M, Gürsoy M, Ismail AF. Development of thin film nanocomposite membrane incorporated with plasma enhanced chemical vapor deposition-modified hydrous manganese oxide for nanofiltration process. Compos B Eng 2019;176:107328.
[55] Ghosh AK, Hoek EMV. Impacts of support membrane structure and chemistry on polyamide-polysulfone interfacial composite membranes. J Membr Sci 2009;336(1–2):140–8.
[56] Deng L, Gonzales RR, Fu W, Xu G, Takagi R, Song Q, et al. Organic solvent separation using carbon nanotube-interlayered thin film composite membrane. Chem Eng J 2023;473:145197.
[57] Hesske H, Gloe K. Hydration behavior of alkyl amines and their corresponding protonated forms. 1. Ammonia and methylamine. J Phys Chem 2007;111(39):9848–53.
[58] Xue W, Tobino T, Nakajima F, Yamamoto K. Seawater-driven forward osmosis for enriching nitrogen and phosphorous in treated municipal wastewater: effect of membrane properties and feed solution chemistry. Water Res 2015;69:120–30.
[59] Bao X, Wu Q, Shi W, Wang W, Zhu Z, Zhang Z, et al. Insights into simultaneous ammonia-selective and anti-fouling mechanism over forward osmosis membrane for resource recovery from domestic wastewater. J Membr Sci 2019;573:135–44.
[60] Kim E-S, Yu Q, Deng B. Plasma surface modification of nanofiltration (NF) thin-film composite (TFC) membranes to improve anti organic fouling. Appl Surf Sci 2011;257(23):9863–71.
[61] Zou L, Vidalis I, Steele D, Michelmore A, Low SP, Verberk JQJC. Surface hydrophilic modification of RO membranes by plasma polymerization for low organic fouling. J Membr Sci 2011;369(1):420–8.
[62] Jhaveri JH, Murthy ZVP. A comprehensive review on anti-fouling nanocomposite membranes for pressure driven membrane separation processes. Desalination 2016;379:137–54.
[63] Chong C-Y, Lau W-J, Yusof N, Lai G-S, Ismail AF. Roles of nanomaterial structure and surface coating on thin film nanocomposite membranes for enhanced desalination. Compos B Eng 2019;160:471–9.
[64] Rana D, Matsuura T. Surface modifications for antifouling membranes. Chemical reviews 2010;110(4):2448–71.
[65] Zhang R, Liu Y, He M, Su Y, Zhao X, Elimelech M, et al. Antifouling membranes for sustainable water purification: strategies and mechanisms. Chem Soc Rev 2016;45(21):5888–924.
[66] Zhao S, Liao Z, Fane A, Li J, Tang C, Zheng C, et al. Engineering antifouling reverse osmosis membranes: a review. Desalination 2021;499:114857.
[67] Gonzales RR, Li J, Zhang P, Xu P, Li Z, Hu M, et al. Hydrogel membrane composite reduces fouling and retains ammonium efficiently. Environ Chem Lett 2024;22:1615–21.
[68] Yuan Y, Hays MP, Hardwidge PR, Kim J. Surface characteristics influencing bacterial adhesion to polymeric substrates. RSC Adv 2017;7(23):14254–61.
[69] Boussu K, Belpaire A, Volodin A, Van Haesendonck C, Van der Meeren P, Vandecasteele C, et al. Influence of membrane and colloid characteristics on fouling of nanofiltration membranes. J Membr Sci 2007;289(1):220–30.
[70] Chen DD, Liu TY, Kang J, Xu RZ, Cao Y, Xiang M. Enhancing the permeability and antifouling properties of polyamide composite reverse osmosis membrane by surface modification with zwitterionic amino acid l-arginine. Adv Mater Interfac 2019;6(14).
[71] Azari S, Zou LD. Using zwitterionic amino acid L-DOPA to modify the surface of thin film composite polyamide reverse osmosis membranes to increase their fouling resistance. J Membr Sci 2012;401:68–75.
[72] Zhang S, Ly QV, Nghiem LD, Wang J, Li J, Hu Y. Optimization and organic fouling behavior of zwitterion-modified thin-film composite polyamide membrane for water reclamation: a comprehensive study. J Membr Sci 2020;596:117748.
[73] Xiao P, Li J, Ren Y, Wang X. A comprehensive study of factors affecting fouling behavior in forward osmosis. Colloids Surf A Physicochem Eng Asp 2016;499:163–72.
[74] Yang Z, Saeki D, Takagi R, Matsuyama H. Improved anti-biofouling performance of polyamide reverse osmosis membranes modified with a polyampholyte with effective carboxyl anion and quaternary ammonium cation ratio. J Membr Sci 2020;595:117529.
[75] Park MJ, Wang C, Seo DH, Gonzales RR, Matsuyama H, Shon HK. Inkjet printed single walled carbon nanotube as an interlayer for high performance thin film composite nanofiltration membrane. J Membr Sci 2021;620:118901.